Lab on a Chip

PAPER

View Article Online
View Journal | View Issue



Cite this: *Lab Chip*, 2014, **14**, 4213

# Siphon-driven microfluidic passive pump with a yarn flow resistance controller†

Gi Seok Jeong,[ab] Jonghyun Oh,‡[a] Sang Bok Kim,[abc] Mehmet Remzi Dokmeci,[ab] Hojae Bae,[g] Sang-Hoon Lee[de] and Ali Khademhosseini*[abcfhi]

Received 30th April 2014,
Accepted 31st July 2014

DOI: 10.1039/c4lc00510d

www.rsc.org/loc

Precise control of media delivery to cells in microfluidic systems in a simple and efficient manner is a challenge for a number of cell-based applications. Conventional syringe pumps can deliver culture media into microfluidic devices at precisely controlled flow rates, but they are bulky and require a power source. On the other hand, passive microflow-generating systems cannot maintain continuous, controllable and long-term delivery of media. We have developed an on-chip microflow control technology that combines flow rate control and passive, long-term delivery of media to microwell tissue culture chambers. Here, a passive flow is initiated using the siphon effect and a yarn flow resistor is used to regulate the flow rate in the microchannel. Using the yarn flow resistor, the medium flow rate into the microfluidic cell culture system is made adjustable to a few hundred microliters per hour. To evaluate the effects of controlled flow on microfluidic cell culture properties (feasibility test), we measured the cell alignment and cytoskeletal arrangement of endothelial cells cultured in a microwell array inside the microfluidic channel.



## Introduction

Continuous and controlled delivery of culture media to cells in microfluidic chips is essential in biomedical applications associated with drug delivery,[1] chemical gradient generation,[2,3] interstitial flow-driven cell migration,[4] or oxygen and nutrient delivery to organs-on-a-chip.[5] The ability to control the flow rate in a cell culture chip within a specific range is crucial because the flow rate can affect the metabolic exchange and shear stress applied to the cells during culture. The interstitial flow ($10^{-1}$–$10^{0}$ μm $s^{-1}$) can increase focal adhesion kinase activation, which is a key factor for migration, sprouting, and alignment among cancer cells.[6] Interstitial flow can also generate protein gradients[7] and deliver diverse cytokines.[8] Furthermore, the flow shear stresses mimicking *in vivo* conditions ($10^{-1}$–$10^{1}$ dyne $cm^{-2}$) can stimulate stem cell differentiation[9–11] and cell alignment.[12–15] Shear stress also plays an important role in the cytoskeletal reorganization of endothelial cells (ECs),[12,13,15] nitric oxide syntheses,[16] and apoptosis inhibition.[17] Therefore, generation of microflow with a flow rate similar to that of physiological-level flow ($10^{-1}$–$10^{1}$ dyne $cm^{-2}$) in microfluidic channels without any use of peripheral devices is critical for mimicking the *in vivo* microenvironment.

Syringe pumps are commonly used to generate and regulate microflows.[18,19] However, continuous delivery of media into microfluidic devices within the cell culture chambers remains challenging since it requires large pumps and a power source. Passive microflow-generating systems, including osmotic pressure-driven micropumps,[2,3] medium reservoir-based flow control systems,[4] and droplet-based surface tension-driven micropumps,[20,21] are also frequently used. However the existing passive systems are limited to short-term uses only, and flow rates are typically not finely adjustable in these systems.

[a] *Biomaterials Innovation Research Center, Division of Biomedical Engineering, Department of Medicine, Brigham and Women's Hospital, Harvard Medical School, Boston, MA 02115, USA. E-mail: alik@rics.bwh.harvard.edu*
[b] *Harvard-MIT Division of Health Sciences and Technology, Massachusetts Institute of Technology, Cambridge, MA 02139, USA*
[c] *Wyss Institute for Biologically Inspired Engineering at Harvard University, Boston, MA 02115, USA*
[d] *Department of Biomedical Engineering, College of Health Science, Korea University, Seoul 136-100, Korea*
[e] *KU-KIST Graduate School of Converging Science and Technology, Korea University, Seoul 136-701, Republic of Korea*
[f] *WPI-Advanced Institute for Materials Research (WPI-AIMR), Tohoku University, 2-1-1 Katahira, Aoba-ku Sendai 980-8577, Japan*
[g] *College of Animal Bioscience and Technology, Department of Bioindustrial Technologies, Konkuk University, Hwayang-dong, Kwangjin-gu, Seoul 143-701, Republic of Korea*
[h] *Department of Maxillofacial Biomedical Engineering and Institute of Oral Biology, School of Dentistry, Kyung Hee University, Seoul 130-701, Republic of Korea*
[i] *Department of Physics, King Abdulaziz University, Jeddah 21569, Saudi Arabia*

† Electronic supplementary information (ESI) available. See DOI: 10.1039/c4lc00510d

‡ Current address: Division of Mechanical Design Engineering, Chonbuk National University, Jeonju, 561-756 Korea

In this paper, we have developed a passive micropump that generates a controllable flow rate similar to the interstitial flow. We employed the siphon effect to initiate the flow and a porous yarn to control the flow rate. The height difference between the upper (inlet) and the lower (outlet) fluid reservoirs created a pressure difference (a driving force), and the force applied by the weight of the water column induced continuous flow. The passive pump system is composed of two reservoirs (inlet and outlet) and a microchannel between the two reservoirs. The flow rate of the micropump was regulated by integrating a piece of yarn into the flow chamber. This yarn acts as a flow resistor to regulate the flow rate. The flow rate was maintained within the range of a few hundred microliters per hour. For the feasibility test, we measured the cell alignment and cytoskeletal arrangement of endothelial cells cultured in a microwell array inside a microfluidic channel in which the controlled flow rate was similar to that of physiological flow.

## Materials and methods

### Principle of the yarn flow resistor (YFR)-based micropump

A yarn flow resistor (YFR) is a flow resistor that utilizes a yarn capillary resistance for siphoning off media in the range of a few hundred microliters per hour. The flow rate in the microchannels without the YFR (channel thickness: 100–300 μm) is maintained in the range of 10–100 mL $h^{-1}$. To maintain the flow rate at the range of a few microliters per day, YFR provides a suitable flow resistance of a siphon-driven passive pump onto a microchannel. The siphon effect is generated by the height difference between the upper (inlet) and lower (outlet) fluid reservoirs, and the fluid moves under the unequal pressures toward the equilibrium configuration[22] (ESI† Fig. S1d). The siphon effect in the presence of the YFR can be described mathematically using the expanded Bernoulli's equation,

$$\frac{1}{2}V_1^2 + gZ_1 + \frac{P_1}{\rho} = \frac{1}{2}V_2^2 + gZ_2 + \frac{P_2}{\rho} + gH_L, \quad (1)$$

where $V$, $Z$, and $P$ indicate the velocity, position, and pressure, respectively. $H_L$ is the total loss of water height due to the channel resistance, and $g$ is the gravitational acceleration constant. $P_1$ and $P_2$ were assumed to be equal to the atmospheric pressure, and the upstream velocity in the reservoir was assumed to be relatively low compared to the velocity at the outlet. Thus, $P_1$, $P_2$, and $V_1$ can be neglected, and $V_2$ in eqn (1) can be expressed as

$$V_2 = [2g(\Delta Z - H_L)]^{1/2} \quad (2)$$

Therefore, the velocity at the outlet depended on the height difference ($\Delta Z$), the resistance due to the YFR, and the channel resistance ($H_L$). The flow rate through a channel equipped with the YFR was determined according to the following equation:

$$Q = \text{YFR outlet area} \times V_{\text{outlet}} = \frac{\pi D_{\text{YFR}}^{\ 2}}{4} \times V_2 \quad (3)$$

Thus, the flow rate through a microfluidic chip with the YFR was determined by calculating the pressure drop ($H_L$). The experimental measurements were used to calculate $H_L$ as shown below,

$$H_L \propto C_{\text{YFR}} \times \text{length of YFR} + \text{base pressure drop}, \quad (4)$$

where $C_{\text{YFR}}$ is the pressure drop constant for the YFR and was calculated to be $2.817 \times 10^{-13}$ $cm^{-1}$. Although the pressure increased with the YFR length, the base head drop contributed the largest amount to the YFR effects. The pressure drop in the channel could be reduced by a few hundred microliters per hour using a short YFR by increasing the porous resistance of the YFR.

### Fabrication of a microfluidic device and a siphon pump

The passive pump was fabricated in a simple, cost-effective manner within a 100 mm × 100 mm square dish. The inlet reservoir and the microchannel are connected by a polyethylene tube (OD = 1.27 mm, ID = 0.86 mm, Instech Laboratories, Inc., PA, USA), and the outlet reservoir and the microchannel are connected with the cotton YFR. The microfluidic channel was fabricated using conventional soft lithography. The poly(dimethylsiloxane) (PDMS; Sylgard 184, Dow Chemical, MI, USA) channel was replicated from the master mold patterned with SU-8 on the silicon wafer (MicroChem, MA, USA). After an oxygen plasma treatment (Femto Science, Korea), the replicated PDMS was bonded to the cover glass.

YFR was fabricated using a cotton yarn (twisted cotton butcher's twine (1 mm × 3 mm), Koch, USA) with a length of approximately 10 cm. YFR was inserted into the tube for easier handling and connection to the microfluidic channel (ESI† Fig. S1a). To connect the reservoir to the microfluidic channel, the tube containing YFR was bent slightly using an alcohol lamp (ESI† Fig. S1b). To initiate siphon-driven flow, a syringe was connected to the outlet of the channel, and a flow was generated from the inlet reservoir to the outlet by drawing up the air in the microchannel with a syringe at the outlet (Fig. 1a and ESI† Fig. S1c). After removing the syringe, we connected the tube containing YFR to the outlet of the microfluidic channel (Fig. 1a, b, and d and ESI† Fig. S1d). The flow initiated from the siphon effect was maintained by the height (and therefore pressure) difference ($\Delta Z$) between the inlet and the outlet medium reservoirs (Fig. 1b) and the fluid flowing through the tubing (R1), the microchannel (R2), and the YFR (R3). Here, the YFR kept the fluid moving at a consistent rate. The fluid flowed continuously through the microchannel until the pressure difference between the inlet and the outlet reservoirs equilibrated ($\Delta Z = 0$). A conical tube (50 mL) was used to connect the inlet reservoir (Fig. 1d) and

 

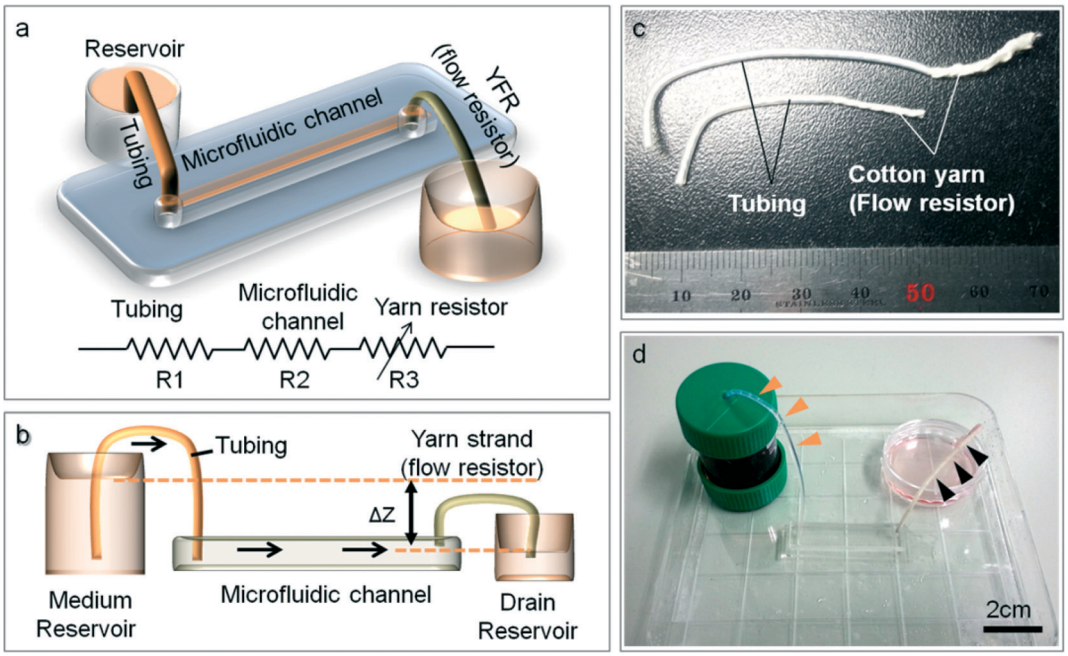


**Fig. 1** YFR-regulated microflow control system. (a) Schematic diagram showing the siphon effects in the yarn capillary resistance-driven micropump system. (b) Schematic diagram of the water head difference-driven siphon effect controlled by the YFR. (c) Photographic image of a yarn capillary regulator. (d) The microfluidic device prepared with a YFR. The system consists of two fluid reservoirs: the microfluidic channels and the YFR (black arrowheads) as well as the drain reservoirs.

the drain tank, a 60 mm diameter Petri dish (Fig. 1d). Flow characteristics were evaluated by measuring the flow rate in a cell incubator to prevent the fluid evaporation from the cotton yarn.

### Human microvascular endothelial cell (hMVEC) culture

hMVECs were purchased from Lonza (Basel, Switzerland) and were cultured in endothelial cell medium (ECM; Sciencell Research Laboratories Inc., CA, USA) consisting of 500 mL of basal medium, 5% fetal bovine serum (FBS), 20 ng $mL^{-1}$ VEGF, and 1% penicillin/streptomycin. The hMVECs were expanded for no more than seven passages. One hundred microliters of a hMVEC suspension ($2 \times 10^5$ cells $mL^{-1}$) was seeded into the microfluidic chip, and the device was placed in a 37 °C incubator overnight to facilitate the attachment of the cells to the cover glass. After cell attachment, the devices were maintained at 37 °C in an incubator (5% $CO_2$). The YFR was connected to the microfluidic device, and the flow was maintained at approximately 3.5 mL per day to induce a shear stress on the hMVECs. The flow rate in the chip was maintained by replenishing the cell culture medium in the reservoir every other day. Cell responses were monitored daily using a phase contrast microscope (AMG, WA, USA).

### Immunocytochemistry

Cells cultured over 48 hours under flow were fixed for 20 min with 4% formaldehyde at 4 °C. For immunostaining, the cells were permeabilized using 0.1% Triton X-100 in 0.1% PBS for 20 min at room temperature and were blocked with 3% BSA in PBS for 30 min followed by incubation in the presence of a primary antibody overnight (4 °C). A primary antibody (Abcam, UK) against α-smooth muscle actin (1 : 1000) was used to observe the cytoskeleton remodelling and cell alignments. After incubating overnight, the cells were washed with PBST (0.05% Tween in PBS) for 5 min. Secondary antibodies (1 : 1000 dilutions, Invitrogen, CA) were applied for 1.5 hours at room temperature. Cells were washed again with PBS, and fluorescence images were acquired using a fluorescence microscope (EVOS, AMG, USA) after counterstaining with 4′,6-diamidino-2-phenylindole dihydrochloride (DAPI, Invitrogen, CA). Cell alignment was measured using the ImageJ software (http://rsbweb.nih.gov/ij/). Statistical analysis was implemented using SPSS version 12 (Chicago, IL, USA).

### Computational analysis in the microfluidic device

The chips were designed to induce a range of shear stresses in two-dimensional (2D) cell culture microchannels prepared with microwell arrays. The chip design is similar to those described in previous studies[30] (ESI† Fig. S2a). The dimensions of the cell culture chip were 1 cm × 3.5 cm, and the height and width of the microchannel were 250 μm and 500 μm, respectively (ESI† Fig. S2a). The shapes formed by the complex flows (velocity and shear stress in the microfluidic channel) were modelled using the finite element method (FEM) implemented in the CFD code (COMSOL Multiphysics 3.4, COMSOL Inc., MA, USA). A triangular grid system was employed for the calculation, and the number of grids was 18 752 (ESI† Fig. S2b). The viscosity of the medium was assumed to be the same as that of water (0.001 Pa s).

The shear stress in the microfluidic channel was calculated based on the results of the CFD analysis. The shear stress ($\tau_c$), the stress imposed on cells attached to the microfluidic channel surface, could be calculated according to

$$\tau_c = \mu \frac{\partial V_o}{\partial y} \quad (5)$$

where $V$ is the velocity of the fluid in the channel. The data were recalculated based on the 2D simulation, taking into account the thickness of the microfluidic channel (ESI† Fig. S2d). For the computational analysis, we performed the mesh sensitivity test of the microfluidic device (ESI† Fig. S2c). We found that the difference of the velocity value is less than 1% between the mesh systems C and D (ESI† Fig. S2c). Finally, we used the mesh system 'C' for the CFD analysis (the number of elements is 18 752).

## Results and discussion

### Characteristics of the yarn flow resistor (YFR)

In our preliminary experiments, the culture medium flow rate was found to be approximately 60 mL $h^{-1}$ through the microchannel (250 μm high, 500 μm wide, and 30 mm long) without the YFR. The siphon pump flow rate needed to be reduced to physiological levels, which could be accomplished using the YFR. Fig. 2 shows the flow characteristics in the microfluidic devices with the YFR. The siphon-induced flow rate in the microchannel was dependent on the height of the reservoir, the length of the YFR, and the dimensions of the microfluidic device. The flow rate increased proportionally with the reservoir height. Fig. 2a shows the flow rate in a microfluidic channel with a height of 500 μm prepared with an 80 ± 3 mm YFR ($n$ = 8). The flow rate clearly increased as the height of the fluid reservoir increased. The flow rate was linearly proportional to the length of the YFR, as shown in Fig. 2b. This result indicates that the YFR length could be a critical factor in the precise control of flow speed in microchannels. Fig. 2c shows the flow rate as a function of the microfluidic channel height. An 80 mm long YFR ($n$ = 8) was used, and the fluid reservoir height was set to 30 mm. Diverse pumping mechanisms can provide diverse ranges of flow rate, and Fig. 2d shows the different flow rates of the different pumping systems. Pneumatic,[23] piezoelectric,[24] osmotic,[3] scanning laser pulse,[25] and electro-active polymer-driven[1] micropump systems have previously been used. The proposed YFR-based micropump produced a continuous flow rate

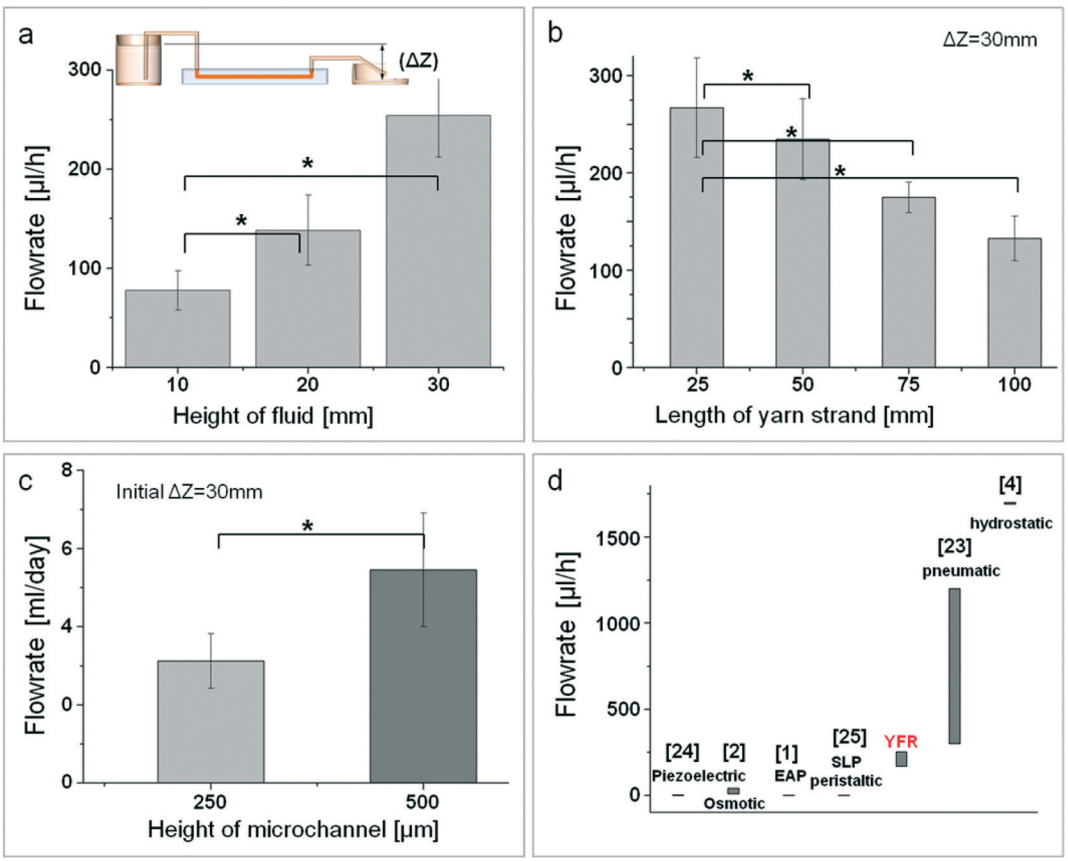


Fig. 2 Quantitative analysis of the YFR flow characteristics. (a) The mean flow rate as a function of the fluid reservoir height prepared using an 80 mm YFR ($n$ = 8). (b) Plot of the mean flow rate as a function of the YFR length for the initial 30 mm reservoir height ($n$ = 8). (c) The mean flow rate in the microfluidic devices prepared using an 80 mm YFR with 250 and 500 μm channel heights ($n$ = 8). (d) Comparison of the flow rates obtained from several types of micropumps. It shows the flow rate range of several micropumping systems including a YFR-based passive pump. A statistical analysis was performed using the $t$-test. The error bars indicate the mean ± standard error (*$P < 0.05$).

 

($\sim 10^2$ μL $h^{-1}$) and shear stress ($\sim 10^{-3}$–$10^{-1}$ dyne $cm^{-2}$), which is an attainable range for a system with a cheap and simple method (Fig. 2a, b, and d).

To date, several devices have been used to provide media to microfluidic cell culturing devices, and conventional syringe pumps and roller-type pumps were typically used. Despite the diverse advantages of these pumps, their extensive applications are limited by the pump size and the power sources for integration to cell culturing incubator systems. Alternatively, several simple and cost-effective passive micropump systems have been developed to facilitate the cell culturing in an incubator.[3,4,6,14] However, these have limits in controlling the flow speed and in long-term operation. The proposed YFR system overcomes these problems. In particular, the fabrication process is simple and cost-effective, and the flow rate and shear stress could be precisely controlled over a broad range.

### Computational analysis of the shear stress and flow direction

Fig. 3 presents the computational results of the fluid flow distribution in the microwell for cell culture under a controllable shear stress. The simulation results illustrate that the recirculation flows in the microwell array were separated from the main flow in the channel (white arrowheads), a typical flow pattern observed in cavities[26,27] (Fig. 3a). The contour plot shows the magnitude of the fluid velocity in the microfluidic device. The red area indicates a region of higher velocity relative to the blue area (Fig. 3a). The arrows indicate the flow direction in the microfluidic device. A clockwise flow was clearly observed in the microwells. The velocity distribution in the microfluidic device is plotted as a function of the *y* position in Fig. 3c (white dotted line in Fig. 3a). The inset shows the recirculation velocity in the microwell area in which the fluid velocity was 100-fold lower than the fluid velocity in the main channel. Although the velocity of interstitial flow has not been elucidated, the order of interstitial flow has been reported within 0.1–2 μm $s^{-1}$.[28–31] Thus, the flow of the YFR-based pump can mimic this interstitial flow level and can be used for the study of cell responses under interstitial flow conditions. Fig. 3d plots the flow-induced shear stress in the microfluidic device. The data were qualitatively and quantitatively similar to the velocity plots. The simulation results supported the utility of the microfluidic device as a cell-culturing platform that can generate a range of shear stress and flow velocities.

### Response of the hMVECs to the flow controlled by the yarn flow resistance

As a proof of concept, we observed the response of the endothelial cells to the *in vivo* level shear stress. The flow pattern

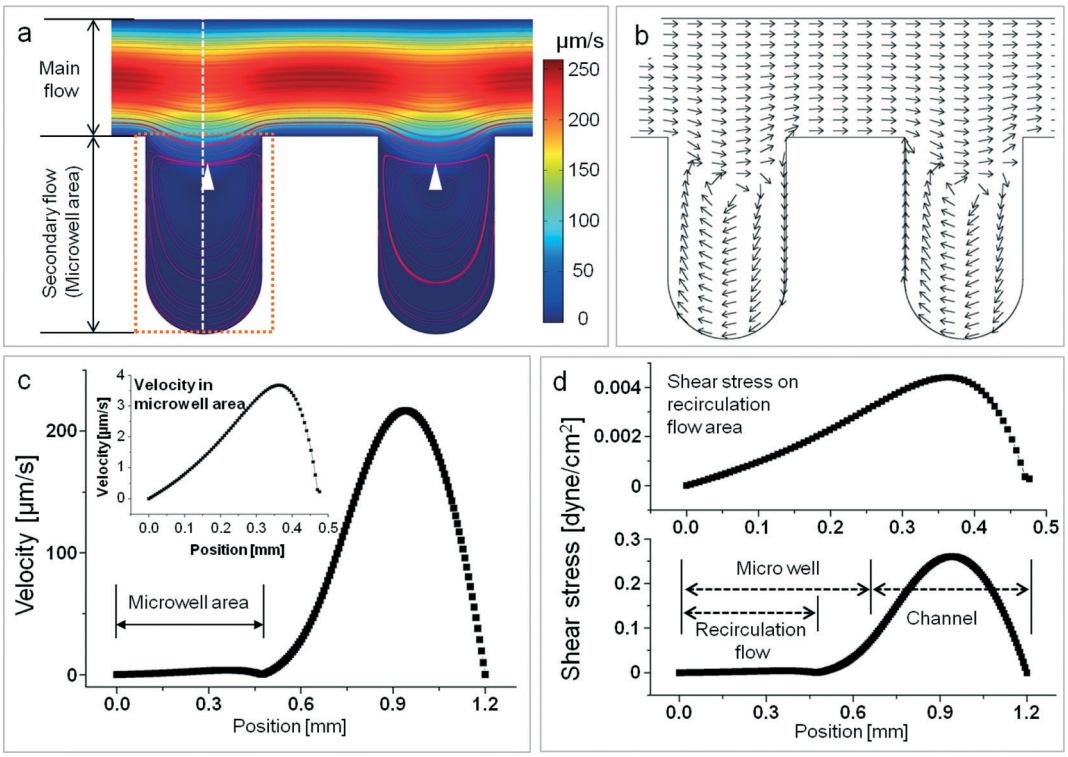


Fig. 3 CFD analysis results obtained from the microfluidic system prepared with an array of microwells. (a) Contour and streamline plots of the microwell array microfluidic channel. Red regions indicate higher flow rates (in the main channel). Separated recirculation flows are indicated by the white arrowheads. Lower flow rates were observed inside the microwells. (b) Arrows indicate the flow direction inside the channel. (c) Graph of the velocity in the microchannel along the white dotted line shown in (a). The inset plots the velocity in the microwell area (orange dotted box). (d) Plot of the shear stress in the microfluidic channel. The data were recalculated based on the 2D simulation with consideration of the microfluidic channel thickness (250 μm).

in the microfluidic channel imposed different levels of shear stress on the cells in the main channel and in the microwell areas over 1 week. The endothelial cell responses to different shear stresses could be observed within a single microfluidic chip using the YFR flow control system. Fig. 4 shows the cells attached in the microfluidic chip (height: 250 μm) under YFR flow control (3 mL per day). In the main channel (with a shear stress of $10^{-1}$ dyne $cm^{-2}$), the attachment area and elongation of the cells were larger than the corresponding values measured in the microwells (with a shear stress of $10^{-3}$ dyne $cm^{-2}$) as shown in the ESI† Fig. S3. The hMVEC alignment on the chip followed the flow streamlines in the main channel (Fig. 4a). The recirculation flow in the microwells appeared to affect the circular arrangement of hMVECs, although its flow rate is much smaller than that in the main channel. These results indicate that the endothelial cells respond to a wide range of slow fluid flow. Fig. 4b and e show a quantitative analysis of the cell morphology under flow-induced shear stress or static conditions. In the main channel, the attachment areas and the cell perimeters were larger than the values measured in the lower shear stress and static areas. The aspect ratios of the cells were also larger in the main channel. The areas and perimeters of the cells under a low shear stress were similar to those measured under static conditions (Fig. 4b). This result suggests that the interstitial flow only affects the direction of hMVEC alignment. The cells grown under a low shear stress ($10^{-3}$ dyne $cm^{-2}$), however, were found to be more elongated than those cultured under static conditions (Fig. 4e). It is well known that the interstitial flow affects cell migration and induces cell elongation.[6,32,33] Fig. 4c and d show that the physiological shear stress levels induced the arrangement of actin stress fibers and altered cell shape. The cell shape and actin fiber patterns were similar to those reported in previous sheared EC studies.[12,13] EC actin filaments grown under static culture conditions were stained, revealing an arrangement along the flow direction. These results support the fact that physiological levels of flow can be regulated by the YFR-based passive micropump system which is more suited to integrated microfluidic devices for long-term cell culturing like organs-on-chips. The areas of the target hMVECs were larger than those measured among hMVECs cultured under static conditions (Fig. 4a, c, and d). The cytoskeleton alignment in the hMVECs grown under shear stress culturing conditions coincided with the direction of the fluid flow. The YFR was useful for the long-term operation and the regulation of microscale fluid flow without the need for any peripheral equipment. The regulated flow rate can

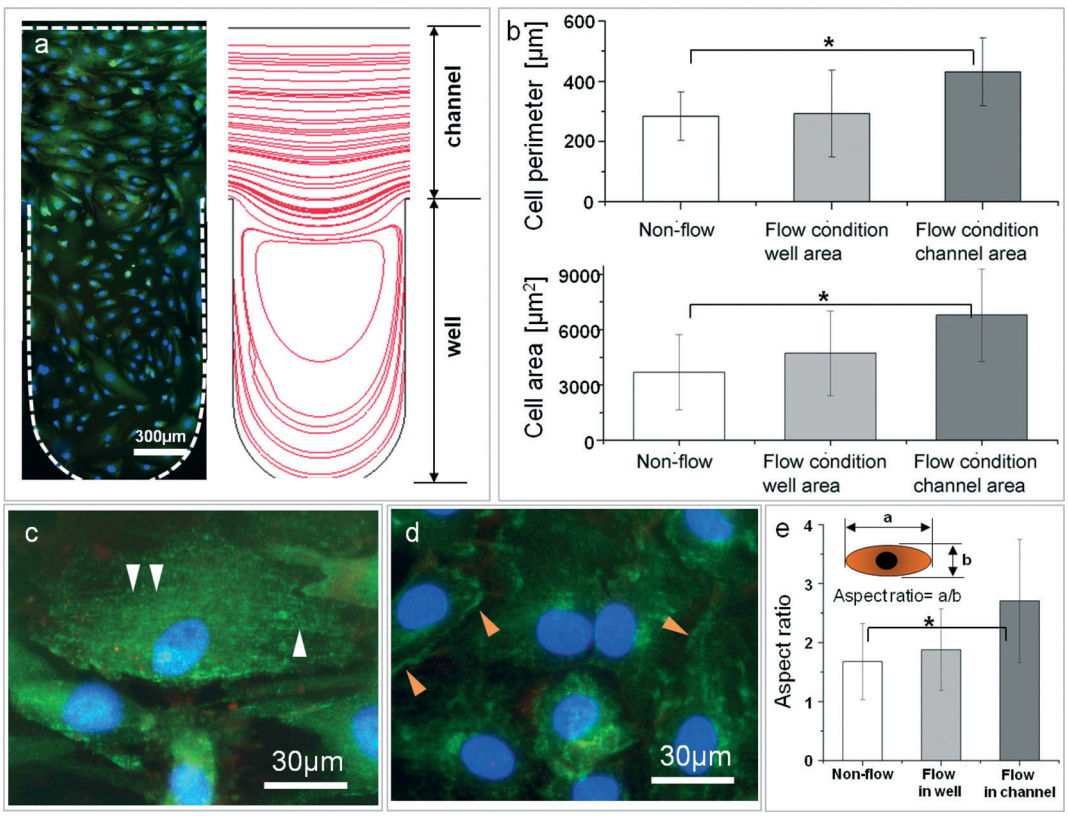


**Fig. 4** Flow-induced endothelial cell response in the microfluidic channel. (a) Comparison of the endothelial alignment and streamlines in the microfluidic channel. The cells were aligned with the flow pattern in the channels. (b) Quantitative analysis of the cell pattern under flow and static conditions. (c) The cytoskeleton arrangement under shear conditions or (d) under static culture conditions. (e) Aspects of the cells cultured under flow or static conditions. The statistical analysis was performed using the paired simple *t*-test. The error bars indicate the mean ± standard error (*$P < 0.05$).

 

consistently generate shear stress in a range that mimics interstitial flow. Such a range of shear stress levels can provide cultured cells with a microenvironment similar to *in vivo* conditions, and the effect of shear stress to endothelial cell properties such as cell alignment, elongation and cytoskeleton alignment can be observed. The proposed system can be extensively used for the quantitative and qualitative investigation of the shear stress effect on diverse cells.

## Conclusions

We have developed a continuous flow-generating pump system using the siphon effect and YFR. The YFR could be easily integrated into a microfluidic channel, and the entire system is simple, cost-effective and small enough to be integrated into a microscale cell culture incubator. Our YFR passive microflow system can mimic *in vivo* conditions in an *in vitro* microscale cell culture incubator. This application is much better than the existing passive microflow pump systems because it allows for precise control of the medium flow rate for continuous, long-term microscale tissue culture. It will enable microfluidic cell culture systems to be much more biomimetic, allowing the development of superior tissue culture and organ on a chip platforms.

## Acknowledgements

This paper is supported by the Korea Research Foundation Grant funded by the Korean Government NRF-2012R1A6A3A03039473.

## References

1 G. H. Kwon, G. S. Jeong, J. Y. Park, J. H. Moon and S. H. Lee, *Lab Chip*, 2011, **11**, 2910–2915.
2 J. Y. Park, C. M. Hwang and S. H. Lee, *Lab Chip*, 2007, **7**, 1673–1680.
3 J. Y. Park, S. J. Yoo, C. M. Hwang and S. H. Lee, *Lab Chip*, 2009, **9**, 2194–2202.
4 O. C. Amadi, M. L. Steinhauser, Y. Nishi, S. Chung, R. D. Kamm, A. P. McMahon and R. T. Lee, *Biomed. Microdevices*, 2010, **12**, 1027–1041.
5 D. Huh, B. D. Matthews, A. Mammoto, M. Montoya-Zavala, H. Y. Hsin and D. E. Ingber, *Science*, 2010, **328**, 1662–1668.
6 W. J. Polacheck, J. L. Charest and R. D. Kamm, *Proc. Natl. Acad. Sci. U. S. A.*, 2011, **108**, 11115–11120.
7 Y. J. Choi, S. Chae, J. H. Kim, K. F. Barald, J. Y. Park and S.-H. Lee, *Sci. Rep.*, 2013, **3**, 1921.
8 S.-A. Lee, E. Kang, J. Ju, D.-S. Kim and S. Lee, *Lab Chip*, 2013, **13**, 3529–3537.
9 K. Yamamoto, T. Takahashi, T. Asahara, N. Ohura, T. Sokabe, A. Kamiya and J. Ando, *J. Appl. Physiol.*, 2003, **95**, 2081–2088.
10 H. Wang, G. M. Riha, S. Yan, M. Li, H. Chai, H. Yang, Q. Yao and C. Chen, *Arterioscler., Thromb., Vasc. Biol.*, 2005, **25**, 1817–1823.
11 T. Ahsan and R. M. Nerem, *Tissue Eng., Part A*, 2010, **16**, 3547–3553.
12 S. G. Eskin, C. L. Ives, L. V. McIntire and L. T. Navarro, *Microvasc. Res.*, 1984, **28**, 87–94.
13 C. G. Galbraith, R. Skalak and S. Chien, *Cell Motil. Cytoskeleton*, 1998, **40**, 317–330.
14 M. Rossi, R. Lindken, B. P. Hierck and J. Westerweel, *Lab Chip*, 2009, **9**, 1403–1411.
15 H. Chen, J. Cornwell, H. Zhang, T. A. Lim, R. Resurreccion, T. Port, G. Rosengarten and R. Nordon, *Lab Chip*, 2013, **13**, 2999–3007.
16 M. Uematsu, Y. Ohara, J. P. Navas, K. Nishida, T. J. Murphy, R. W. Alexander, R. M. Nerem and D. G. Harrison, *Am. J. Physiol.*, 1995, **269**, C1371–C1378.
17 S. Dimmeler, J. Haendeler, V. Rippmann, M. Nehls and A. M. Zeiher, *FEBS Lett.*, 1996, **399**, 71–74.
18 P. J. Hung, P. J. Lee, P. Sabounchi, N. Aghdam, R. Lin and L. P. Lee, *Lab Chip*, 2004, **5**, 44–48.
19 S. R. Quake, *Anal. Chem.*, 2007, **79**, 8557–8563.
20 E. Berthier and D. J. Beebe, *Lab Chip*, 2007, **7**, 1475–1478.
21 J. Ju, J. Y. Park, K. C. Kim, H. Kim, E. Berthier, D. J. Beebe and S.-H. Lee, *J. Micromech. Microeng.*, 2008, **18**, 087002.
22 J. Steigert, T. Brenner, M. Grumann, L. Riegger, S. Lutz, R. Zengerle and J. Ducree, *Biomed. Microdevices*, 2007, **9**, 675–679.
23 J. Y. Kim, J. Y. Baek, K. H. Lee, Y. D. Park, K. Sun, T. S. Lee and S. H. Lee, *Lab Chip*, 2006, **6**, 1091–1094.
24 S. Ford and S. Soper, *Analyst*, 1998, **123**, 1435–1441.
25 Y. Chen, T.-H. Wu and P.-Y. Chiou, *Lab Chip*, 2012, **12**, 1771–1774.
26 S. Hou, Q. Zou, S. Chen, G. Doolen and A. C. Cogley, *J. Comput. Phys.*, 1995, **118**, 329–347.
27 O. Botella and R. Peyret, *Comput. Fluids*, 1998, **27**, 421–433.
28 S. R. Chary and R. K. Jain, *Proc. Natl. Acad. Sci. U. S. A.*, 1989, **86**, 5385–5389.
29 R. K. Jain, *Annu. Rev. Biomed. Eng.*, 1999, **1**, 241–263.
30 H. Dafni, T. Israely, Z. M. Bhujwalla, L. E. Benjamin and M. Neeman, *Cancer Res.*, 2002, **62**, 6731–6739.
31 M. A. Swartz and M. E. Fleury, *Annu. Rev. Biomed. Eng.*, 2007, **9**, 229–256.
32 A. R. Wechezak, R. F. Viggers and L. R. Sauvage, *Lab. Invest.*, 1985, **53**, 639–647.
33 U. Haessler, J. C. M. Teo, D. Foretay, P. Renaud and M. A. Swartz, *Integr. Biol.*, 2012, **4**, 401–409.